Journal of Sound and Vibration (2000) **234**(5), 761–775
doi:10.1006/jsvi.1999.2861, available online at http://www.idealibrary.com on IDEAL®

TRAILING EDGE NOISE AT LOW MACH NUMBERS, PART 2: ATTACHED AND SEPARATED EDGE FLOWS

M. S. Howe

College of Engineering, Boston University, 110 *Cummington Street, Boston MA* 02215, *U.S.A.*

(*Received* 26 *March* 1999, *and in final form* 30 *November* 1999)

The diffraction theory of Part 1 [1] for estimating the sound generated by low Mach number flow past the trailing edge of an airfoil of compact, but finite thickness is applied to investigate the noise produced by turbulent flow over an edge whose upper surface profile (the suction side) is rounded. The sound is expressed in terms of the "upwash" velocity fluctuations that the same boundary layer turbulence would generate if the airfoil were absent. An approximate method is proposed for expressing these fluctuations in terms of local properties of the blocked pressure generated on the surface exposed to the turbulent flow. Predictions are made of the edge-noise spectrum for both fully attached flow (that remains attached right up to the trailing edge) and for cases where separation occurs on the rounded profile. When premature separation occurs the amplitude of the edge-generated sound decreases exponentially with increasing frequency, and predicted edge-noise levels are significantly smaller than estimates obtained when the airfoil is modelled by a rigid half-plane. For attached flow turbulence on the suction side of the airfoil always passes close to the edge and interacts strongly with it, but contributions from the interaction of the same turbulence with the pressure side of the airfoil are reduced because of the finite airfoil thickness. In this case sound levels fall short of those for a rigid half-plane typically by about 5–10 dB, the precise values being dependent on frequency, and on the ratio of the boundary layer thickness to the mean airfoil thickness.

1. INTRODUCTION

Consider turbulent flow at very small Mach number over the upper surface of the trailing edge of an uncambered airfoil with a rounded upper surface edge profile, as illustrated in Figure 1. The profile is the same for all spanwise locations, so that the edge is parallel to the airfoil span. Airfoils of this type are frequently used in flow noise tests [2–4], and the simplified edge geometry is convenient for validating numerical codes for edge-noise prediction. Let the main stream outside the airfoil boundary layers have low subsonic speed U in the x_1 direction of the rectangular co-ordinate axes (x_1, x_2, x_3). The co-ordinate origin O lies on the midplane of the airfoil in the "vertical" plane of the trailing edge A (see Figure 2(a)). The upper, rounded edge region extends over the interval $-\ell < x_1 < 0$, and meets the lower surface at A: $x_1 = 0$, $x_2 = -\frac{1}{2}h$. Upstream of the edge, for $x_1 < \ell$, the airfoil has uniform thickness h and its upper and lower surfaces coincide with the planes $x_2 = \pm\frac{1}{2}h$. The mean circulation around the airfoil is assumed to be adjusted to make A a stagnation point.

The theory of the self-noise generated at a trailing edge of finite thickness was discussed in Part 1 [1], which also includes a brief review of earlier theoretical work. When the airfoil

0022-460X/00/300761 + 15 $35.00/0

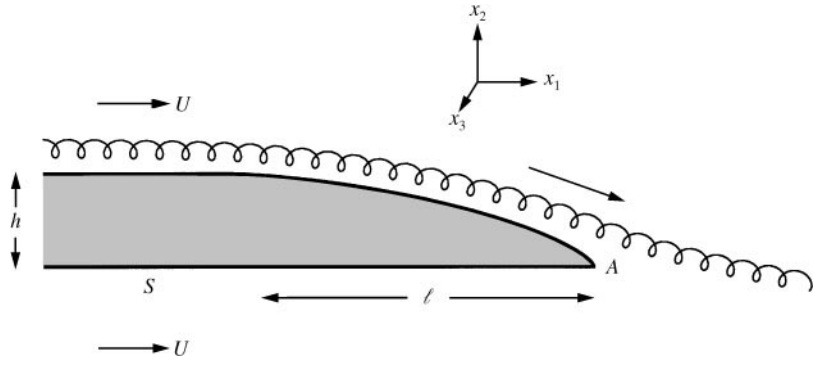

Figure 1. Schematic low Mach number turbulent boundary layer flow over a rounded trailing edge.

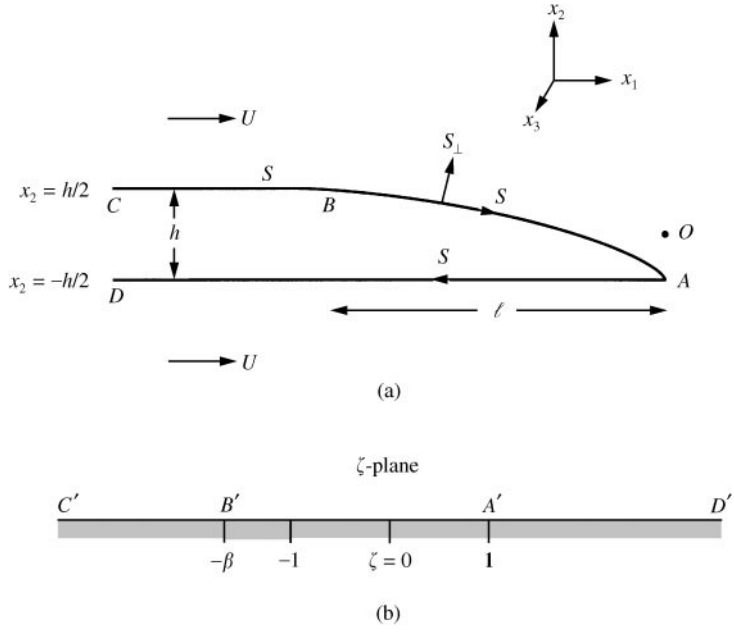

Figure 2. (a) Configuration of the trailing edge and the coordinate system. (b) Mapping the region outside the airfoil (in the plane of $z = x_1 + ix_2$) onto the upperhalf of the ζ-plane.

thickness h is acoustically compact, it was shown that the acoustic pressure $p(\mathbf{x}, t)$ in the far field at $\mathbf{x}$ at time t can be rendered in the form

$$p(\mathbf{x}, t) = \int_{-\infty}^{\infty} p(\mathbf{x}, \omega) \mathrm{e}^{-\mathrm{i}\omega t} \, \mathrm{d}\omega, \tag{1}$$

$$p(\mathbf{x}, \omega) \approx \frac{\rho_0 \kappa_0^{1/2} \sin^{1/2}\psi \sin(\theta/2) \mathrm{e}^{\mathrm{i}\kappa_0 |\mathbf{x}|}}{\pi \sqrt{2\pi \mathrm{i}} |\mathbf{x}|} \oint_S \left\{ \mathrm{i}\omega \Phi^*(\mathbf{y}) v_{\mathbf{I}n}(\mathbf{y}, \omega) + v \boldsymbol{\Omega}(\mathbf{y}, \omega) \wedge \frac{\partial \Phi^*(\mathbf{y})}{\partial \mathbf{y}} \cdot \mathbf{n} \right\} \mathrm{d}S(\mathbf{y}),$$

$$|\mathbf{x}| \to \infty, \tag{2}$$

where the integration is over the upper and lower surfaces S of the airfoil. The terms in this formula are defined as

$$\begin{aligned} \rho_0 &= \text{mean fluid density}, \\ \kappa_0 &= \omega/c_0 = \text{acoustic wavenumber}, \\ c_0 &= \text{speed of sound}, \\ \nu &= \text{kinematic viscosity}, \\ \mathbf{\Omega} &= \operatorname{curl} \mathbf{v} = \text{vorticity}, \ \mathbf{v} = \text{velocity}, \\ \sin\psi &= r/|\mathbf{x}|, \qquad r = \sqrt{x_1^2 + x_2^2}, \\ \sin\theta &= x_2/r. \end{aligned} \tag{3}$$

Thus, $(x_1, x_2) = r(\cos\theta, \sin\theta)$, and ψ is the angle between the radiation direction $\mathbf{x}/|\mathbf{x}|$ and the x_3-axis (the airfoil span, out of the plane of the paper in Figure 1).

$\Phi^*(\mathbf{x}) = \Phi^*(x_1, x_2)$ is an auxiliary function that depends on the shape of the airfoil trailing edge profile. It satisfies Laplace's equation and describes an incompressible, irrotational flow around the edge of the airfoil (in planes parallel to the x_1x_2-plane), and is normalized such that

$$\Phi^*(x_1, x_2) \to \varphi^*(x_1, x_2) \equiv \sqrt{r}\sin(\theta/2) \quad \text{for } \sqrt{x_1^2 + x_2^2} \gg h, \tag{4}$$

where $\varphi^*(x_1, x_2)$ is the corresponding potential of irrotational flow (in the anticlockwise direction) about the edge of the *half-plane* $x_1 < 0$, $x_2 = 0$.

The unit normal on S directed into the fluid is denoted by $\mathbf{n}$, and $v_{In} = \mathbf{v}_\mathbf{I} \cdot \mathbf{n}$ is the normal component of the "upwash velocity". This is defined by

$$\frac{\partial \mathbf{v}_\mathbf{I}}{\partial t} = -\operatorname{curl} \int_V \frac{\operatorname{curl}(\mathbf{\Omega} \wedge \mathbf{v})\, \mathrm{d}^3\mathbf{y}}{4\pi|\mathbf{x} - \mathbf{y}|} \equiv \operatorname{curl} \int_V \left(\frac{\partial \mathbf{\Omega}}{\partial t} - \nu \nabla^2 \mathbf{\Omega} \right) \frac{\mathrm{d}^3 y}{4\pi|\mathbf{x} - \mathbf{y}|}, \tag{5}$$

where V is the region occupied by the fluid. The vortical boundary layer motion is assumed to be well approximated at low Mach numbers by the Navier–Stokes equation for *incompressible* flow. In the viscous sublayer, close to the surface of the airfoil, the motion becomes *linear* and

$$\frac{\partial \mathbf{\Omega}}{\partial t} - \nu \nabla^2 \mathbf{\Omega} \approx \mathbf{0}.$$

Outside the sublayer viscous diffusion is negligible, and $\nu \nabla^2 \mathbf{\Omega}$ may be discarded from the second integrand of equation (5). The upwash velocity is then given by the Biot–Savart formula [5]

$$\mathbf{v}_\mathbf{I}(\mathbf{x}, t) = \operatorname{curl} \int_{V_0} \frac{\mathbf{\Omega}(\mathbf{y}, t)\, \mathrm{d}^3\mathbf{y}}{4\pi|\mathbf{x} - \mathbf{y}|}, \tag{6}$$

where the integration is confined to the non-linear region of the boundary layer V_δ *outside* the viscous sublayer. This result implies that, in applications to flows of very large Reynolds numbers, where the dominant turbulent motions may be regarded as essentially inviscid, possible contributions to the integral (6) from *potential flow bound vorticity* on S must be excluded.

Equation (6) defines the velocity $\mathbf{v}_\mathbf{I}$ in terms of the boundary layer vorticity *when the presence of the airfoil is ignored*, i.e., when the volume enclosed by S is imagined to contain fluid moving irrotationally at the induced velocity of the boundary layer vorticity. Of course, prior to evaluating the upwash velocity from either of the representations (5) or (6), the vorticity $\boldsymbol{\Omega}(\mathbf{x}, t)$ and flow velocity $\mathbf{v}(\mathbf{x}, t)$ must first be determined with full account taken of the presence of the airfoil and of the no-slip condition on S.

The first term in the brace brackets of the integrand of equation (2) represents the contribution to the edge noise from the *normal* surface stresses on S; the second term determines the net contribution from the surface shear stress, and is usually neglected at very high Reynolds numbers [1].

In Part 1, the two-dimensional version of equation (2) was used to examine the sound generated during the mean flow convection of a rectilinear vortex past the trailing edge of Figure 1, including the influence of vortex shedding induced from the edge A. In this paper, equation (2) will be applied to estimate the acoustic pressure frequency spectrum of the high-frequency self-noise generated by turbulent flow over the rounded edge profile. The theory is formulated (in section 2) to enable account to be taken of changes in the mean turbulent boundary layer characteristics with distance from the edge. In the theory of edge noise generated by flow over the edge of a thin plate airfoil [6–8], the properties of the boundary layer turbulence are expressed in terms of the blocked wall pressure wavenumber–frequency spectrum, measured or specified empirically just upstream of the edge. In the present formulation (section 3) it is assumed that the relevant frequencies are sufficiently high such that the wavenumber–frequency spectrum of the *upwash velocity* $v_{\mathbf{I}n}$ can be represented locally in terms of the blocked pressure spectrum, thereby permitting acoustic predictions to be made in terms of measured or calculated turbulence parameters. The Mach number is sufficiently small such that the blocked pressure can be calculated from the incompressible equations of motion. Numerical results are presented in section 3 for fully attached and separated edge flows, including a comparison with predictions of the *frozen* approximation of references [6–8], according to which the boundary layer turbulence is convected over the edge along a path parallel to the undisturbed mean stream.

2. FORMAL REPRESENTATION OF THE EDGE NOISE

Introduce a curvilinear co-ordinate system $(s, s_\perp, x_3)$, where s is measured along the curvilinear stream lines of the potential function $\Phi^*(x_1, x_2)$ in the clockwise direction, $s_\perp$ lies in the x_1x_2-plane, normal to the streamlines and directed *away* from the profile S of the airfoil, on which we can take $s_\perp = 0$ (Figure 2(a)). Then $s_\perp > 0$ in the fluid, and on S,

$$v_{\mathbf{I}n} = \lim_{s_\perp \to -0} \frac{\partial \Phi}{\partial s_\perp}(s, s_\perp, x_3, \omega) \equiv \lim_{s_\perp \to -0} \frac{\partial}{\partial s_\perp} \int_{-\infty}^{\infty} \hat{\Phi}(s, s_\perp, k_3, \omega) \mathrm{e}^{\mathrm{i}k_3 x_3} \, \mathrm{d}k_3, \tag{7}$$

where $\Phi(s, s_\perp, x_3, \omega)$, $\hat{\Phi}(s, s_\perp, k_3, \omega)$ are, respectively, the upwash velocity potential and its Fourier transform with respect to x_3. This potential is well defined throughout the whole of space where the vorticity $\boldsymbol{\Omega} = \mathbf{0}$, including the region occupied by the airfoil.

When the final representation in equation (7) is substituted for v_{1n} in equation (2), with $dS = ds\,dy_3$, the integration with respect to y_3 yields the delta function $\delta(k_3)$. In an *exact* integral representation of the edge-generated sound (involving the specification of *compressible* data on S) the surface integral would actually yield $\delta(k_3 - \kappa_0 \cos\psi)$, which merely implies that only those Fourier components of $v_{1n}(s, x_3, \omega)$ that have supersonic spanwise phase velocity $|\omega/k_3| > c_0$ are responsible for the radiation of sound from the edge. In other words, the only relevant wavenumbers are confined to the *acoustic domain* $|k_3| < |\kappa_0|$, and correspond to variations in the spanwise direction occurring over distances of the order of the acoustic wavelength. However, the dominant hydrodynamic motions near the edge have length scales of the order of the boundary layer displacement thickness $\delta^* \ll 1/\kappa_0 < 1/|k_3|$. In the approximation of equation (2), $\kappa_0\delta^*$ is so small that we can take $k_3 = 0$.

When $k_3 = 0$ and the source motion is regarded as incompressible, the velocity potential $\hat{\Phi}(s, s_\perp, k_3, \omega)$ satisfies Laplace's equation, which locally reduces to

$$\left(\frac{\partial^2}{\partial s^2} + \frac{\partial^2}{\partial s_\perp^2}\right) \Phi(s, s_\perp, 0, \omega) = 0.$$

The corresponding *stream function* $\hat{\Psi}(s, s_\perp, \omega)$, say, is related to $\hat{\Phi}(s, s_\perp, 0, \omega)$ by the Cauchy–Riemann equations [5]

$$\frac{\partial \hat{\Psi}}{\partial s} = -\frac{\partial \hat{\Phi}}{\partial s_\perp}(s, s_\perp, 0, \omega), \qquad \frac{\partial \hat{\Psi}}{\partial s_\perp} = \frac{\partial \hat{\Phi}}{\partial s}(s, s_\perp, 0, \omega). \tag{8}$$

Hence, substituting from equation (7) into equation (2), and discarding the contribution to the radiation from the surface shear stress, we find

$$p(\mathbf{x}, \omega) \approx \frac{\rho_0 \omega}{|\mathbf{x}|}\sqrt{\frac{2i\kappa_0}{\pi}}\sin^{1/2}\psi \sin(\theta/2) e^{i\kappa_0|\mathbf{x}|}\int_{-\infty}^{\infty} \Phi^*(\mathbf{y}(s))\left(\frac{\partial \hat{\Phi}}{\partial s_\perp}(s, s_\perp, 0, \omega)\right)_{s_\perp = 0} ds$$

$$= \frac{-\rho_0 \omega}{|\mathbf{x}|}\sqrt{\frac{2i\kappa_0}{\pi}}\sin^{1/2}\psi \sin(\theta/2) e^{i\kappa_0|\mathbf{x}|}\int_{-\infty}^{\infty} \Phi^*(\mathbf{y}(s))\frac{\partial \hat{\Psi}}{\partial s}(s, 0, \omega)\, ds, \quad |\mathbf{x}| \to \infty, \tag{9}$$

where the integration is taken in the clockwise sense around the profile $s_\perp = 0$ of the airfoil S.

Since the noise sources are confined to the neighborhood of the trailing edge, we may integrate by parts in the final line of equation (9) to express the radiation as a Stieltjes integral

$$p(\mathbf{x}, \omega) \approx \frac{\rho_0 \omega}{|\mathbf{x}|}\sqrt{\frac{2i\kappa_0}{\pi}}\sin^{1/2}\psi \sin(\theta/2) e^{i\kappa_0|\mathbf{x}|}\oint_S \hat{\Phi}(s, 0, \omega)\, d\Phi^*, \quad |\mathbf{x}| \to \infty, \tag{10}$$

where the integration is in the clockwise direction about S. In section 3 it will be convenient to evaluate the integral by setting $z = x_1 + ix_2$, and mapping the region of the z-plane outside the airfoil occupied by the fluid onto the upper half of the complex ζ-plane, such that the airfoil profile S transforms into the real ζ-axis with the correspondence of boundary points indicated in Figure 2(b). But, the potential Φ^* is given in terms of ζ by

$$\Phi^* \equiv \Phi^*(z) = -\mu \mathrm{Re}\,\zeta, \quad \mu > 0, \tag{11}$$

where μ is a constant whose value depends on the shape of the trailing edge profile. Thus, the acoustic pressure may be written as

$$p(\mathbf{x}, \omega) \approx -\frac{\rho_0 \mu \omega}{|\mathbf{x}|}\sqrt{\frac{2\mathrm{i}\kappa_0}{\pi}}\sin^{1/2}\psi \sin(\theta/2)\mathrm{e}^{\mathrm{i}\kappa_0|\mathbf{x}|}\int_{-\infty}^{\infty}\hat{\Psi}^*(s(\zeta), 0, \omega)\,\mathrm{d}\zeta, \quad |\mathbf{x}| \to \infty, \quad (12)$$

where the path of integration runs just above any singularities on the real axis.

3. MODELLING HIGH-FREQUENCY EDGE NOISE

3.1. CONFORMAL MAPPING

The fluid region bounded internally by a trailing edge profile of the type shown in Figure 2(a) is mapped into the upper ζ-plane by means of the transformation [1]

$$\frac{z}{h} = \frac{1}{(1+\alpha)}[\, f(\zeta, 1) + \alpha f(\zeta, \beta)], \quad \alpha > 0, \beta > +1, \quad (13)$$

where α and β are numerical constants, and

$$f(\zeta, \beta) = -\frac{4}{\pi(1+\beta)2}\left(\zeta + \frac{\beta - 1}{2}\right)\sqrt{\zeta + \beta}\sqrt{\zeta - 1}$$
$$+ \frac{1}{\pi}\ln\left[\left(\zeta + \frac{\beta - 1}{2}\right) + \sqrt{\zeta + \beta}\sqrt{\zeta - 1}\right] - \frac{\mathrm{i}}{2} - \frac{1}{\pi}\ln\left(\frac{1+\beta}{2}\right). \quad (14)$$

Equation (13) maps the real ζ-axis (Figure 2(b)) onto an airfoil profile S whose upper and lower surfaces coincide with $x_2 = \pm\frac{1}{2}h$, respectively, for $\mathrm{Re}\,\zeta < -\beta$ and $\mathrm{Re}\,\zeta > 1$. This transformation divides the upper, rounded section of the trailing edge (between B and A in Figure 2(a)) in two sections: the interval $-\beta < \mathrm{Re}\,\zeta < -1$ is the image of the section that starts at B and terminates (at $\zeta = -1$) at the top of a vertical "end-face" ($x_1 = 0$, $-\frac{1}{2}h < x_2 < -\frac{1}{2}h + \Delta$) of thickness Δ, which corresponds to the interval $-1 < \mathrm{Re}\,\zeta < 1$. The values of α and β are calculated by prescribing values for the geometrical ratios ℓ/h and Δ/h. As in Part 1, results presented in this paper are for

$$\alpha = 600, \qquad \beta = 86{\cdot}9370 \quad (15)$$

which yield $\ell/h = 4$ and $\Delta/h = 0{\cdot}0074$. The corresponding airfoil profile is shown in Figure 2(a) (because $\Delta \ll h$ the end-face cannot be distinguished).

The coefficient μ in the definition (11) of Φ^* is determined from condition (4), which is equivalent to $-\mu\zeta \to -\mathrm{i}\sqrt{z}$ as $|z|/h \to \infty$, and supplies

$$\mu = \sqrt{\frac{h}{\pi(1+\alpha)}\left(1 + \frac{4\alpha}{(1+\beta)^2}\right)}. \quad (16)$$

3.2. THE FROZEN APPROXIMATION

In the *frozen approximation* of thin airfoil theory [6–8] the boundary layer turbulence is assumed to convect parallel to the undisturbed mean stream at a convection velocity U_c,

which depends weakly on frequency ω. When this is applied to the airfoil of Figure 2(a), boundary layer eddies translate as frozen distributions of vorticity in the x_1 direction within a boundary layer constrained to lie above the plate in the $x_2 > \frac{1}{2}h$, so that the separation streamline is parallel to the undisturbed mean flow velocity, and extends downstream parallel to the x_1-axis. $\hat{\Psi}$ satisfies Laplace's equation in the region $x_2 \leqslant \frac{1}{2}h$, where we can write

$$\hat{\Psi}(x_1, x_2, \omega) = \int_{-\infty}^{\infty} \mathscr{A}(k, \omega) \mathrm{e}^{\mathrm{i}kx_1 - |k|(h/2 - x_2)} \, \mathrm{d}k, \quad x_2 \leqslant \frac{1}{2} h. \tag{17}$$

It was shown in Part 1 (section 3.2) that the pressure fluctuations $p_I(\mathbf{x}, t)$ in the region $x_2 \leqslant \frac{1}{2}h$ that would be produced by the boundary layer turbulence *if the presence of the airfoil is ignored* satisfies the linear relation $\partial \mathbf{v_I}/\partial t = (-1/\rho_0) \nabla p_I$, and it therefore follows by applying this relation on $x_2 \sim \frac{1}{2}h$ that

$$\mathscr{A}(k, \omega) = \frac{\mathrm{sgn}(k)}{2\rho_0 \omega} p_s(k, 0, \omega), \tag{18}$$

$p_s(k, k_3, \omega)$ being the Fourier transform of the blocked wall pressure, defined by

$$p_s(k, k_3, \omega) = \frac{1}{(2\pi)^3} \int_{-\infty}^{\infty} p_s(x_1, x_3, t) \mathrm{e}^{-\mathrm{i}\{kx_1 + k_3 x_3 - \omega t\}} \, \mathrm{d}x_1 \, \mathrm{d}x_3 \, \mathrm{d}t, \tag{19}$$

where $p_s(x_1, x_3, t) \equiv 2p_\mathrm{I}(x_1, h/2, x_3, t)$ is the pressure that would be exerted by the boundary layer on a rigid wall at $x_2 = \frac{1}{2}h$, i.e., on the upstream, flat section of the upper surface of the airfoil. In the frozen approximation it is assumed that measurements of $p_s(x_1, x_3, t)$ several characteristic hydrodynamic length scales upstream of the trailing edge are sufficient to determine $p_s(k, k_3, \omega)$.

Then, in equation (12) we find

$$\int_{-\infty}^{\infty} \hat{\Psi}(s(\zeta), 0, \omega) \, \mathrm{d}\zeta = \frac{1}{2\rho_0 \omega} \int_{-\infty}^{\infty} \mathscr{I}(k) p_s(k, 0, \omega) \, \mathrm{d}k, \tag{20}$$

$$\mathscr{I}(k) = \begin{cases} \text{c.c.} \{ \mathrm{e}^{-kh/2} \int_{-\infty}^{\infty} \mathrm{e}^{-\mathrm{i}kz} \, \mathrm{d}\zeta \} & \text{for } k > 0, \\ -\text{c.c.} \{ \mathscr{I}(-k) \} & \text{for } k < 0, \end{cases} \tag{21}$$

where "c.c." denotes the complex conjugate. Thus, equations (12) and (1) give the farfield sound in the form

$$p(\mathbf{x}, t) \approx -\frac{\mu \sin^{1/2} \psi \sin(\theta/2)}{\sqrt{2\pi c_0} |\mathbf{x}|} \iint_{-\infty}^{\infty} \omega^{1/2} \mathscr{I}(k) p_s(k, 0, \omega) \mathrm{e}^{-\mathrm{i}\omega(t - |\mathbf{x}|/c_0) + \mathrm{i}\pi/4} \, \mathrm{d}k \, \mathrm{d}\omega, \quad |\mathbf{x}| \to \infty. \tag{22}$$

The acoustic pressure frequency spectrum $\Phi(\mathbf{x}, \omega)$, which satisfies

$$\langle p^2(\mathbf{x}, t) \rangle = \int_0^{\infty} \Phi(\mathbf{x}, \omega) \, \mathrm{d}\omega,$$

the angle brackets $\langle\ \rangle$ denoting an ensemble average, is calculated from equation (22) by first assuming that only a finite spanwise section $-\frac{1}{2}L < x_3 < \frac{1}{2}L$ of the trailing edge is wetted by the turbulent flow, where L is much larger than the boundary layer thickness δ. For statistically stationary turbulence,

$$\langle p_s(k, 0, \omega) p_s^*(k', 0, \omega')\rangle \approx \frac{L}{2\pi}\delta(\omega - \omega')\delta(k - k')P(k, 0, \omega), \quad L \gg \delta, \tag{23}$$

where the asterisk represents the complex conjugate, and $P(k, k_3, \omega) \equiv P(-k, k_3, -\omega)$ is the wavenumber–frequency spectrum of the blocked wall pressure [9]. Then equation (22) yields

$$\Phi(\mathbf{x}, \omega) = \frac{\mu^2 \sin\psi \sin^2(\theta/2)}{2\pi^2|\mathbf{x}|^2}\frac{\omega L}{c_0}\int_{-\infty}^{\infty} |\mathscr{I}(k)|^2 P(k, 0, \omega)\,\mathrm{d}k, \quad |\mathbf{x}| \to \infty. \tag{24}$$

To illustrate predictions of this formula the wall-pressure spectrum will be approximated by the Corcos formula, which is applicable for $\omega\delta/U > 1$ in the immediate neighborhood of the "convective ridge" (where $P(k, k_3, \omega)$ attains a large maximum) [10]:

$$P(k, k_3, \omega) = \Phi_{pp}(\omega)\frac{\ell_1}{\pi[1 + \ell_1^2(k - \omega/U_c)^2]}\frac{\ell_3}{\pi[1 + \ell_3^2 k_3^2]},$$

$$\ell_1 \approx 9U_c/\omega, \qquad \ell_3 \approx 1{\cdot}4U_c/\omega, \qquad U_c \approx 0{\cdot}7U. \tag{25}$$

The lengths ℓ_1 and ℓ_3 are frequency-dependent turbulence correlation scales in the x_1 and x_3 directions. Φ_{pp} is the *point pressure frequency spectrum* which will be approximated by the following empirical formula (based on data collected by Chase [9]):

$$\frac{(U/\delta_*)\Phi_{pp}(\omega)}{(\rho_0 v_*^2)^2} = \frac{(\omega\delta_*/U)^2}{[(\omega\delta_*/U)^2 + \alpha_p^2]^{3/2}}, \qquad \alpha_p = 0{\cdot}12, \tag{26}$$

where $\delta_* \sim \delta/8$ is the boundary layer displacement thickness, and v_* is the friction velocity.

The principal contribution to the integral in equation (24) is from the immediate vicinity of the spectral maximum in the convective ridge, where $k \sim \omega/U_c$. We therefore replace $\mathscr{I}(k)$ by $\mathscr{I}(\omega/U_c)$ to obtain

$$\Phi(\mathbf{x}, \omega) \approx \frac{\mu^2 \sin\psi \sin^2(\theta/2)}{2\pi^2|\mathbf{x}|^2}\frac{\omega L}{c_0}\left|\mathscr{I}\left(\frac{\omega}{U_c}\right)\right|^2\int_{-\infty}^{\infty} P(k, 0, \omega)\,\mathrm{d}k$$

$$\approx \frac{0{\cdot}7LM_c\mu^2 \sin\psi \sin^2(\theta/2)}{\pi^3|\mathbf{x}|^2}\left|\mathscr{I}\left(\frac{\omega}{U_c}\right)\right|^2\Phi_{pp}(\omega), \quad |\mathbf{x}| \to \infty, \tag{27}$$

where the $M_c = U_c/c_0$ is the convection Mach number.

The integral in equation (21) defining $\mathscr{I}(k)$ must be evaluated numerically, with $z = z(\zeta)$ *determined by equation* (13). *Then the acoustic frequency spectrum can be expressed in the non-dimensional form*

$$\frac{(U/\delta_*)\Phi(\mathbf{x},\omega)}{(\rho_0 v_*^2)^2} \approx \mu^2 M \left(\frac{L\delta_*}{|\mathbf{x}|^2}\right) \sin\psi \sin^2\left(\frac{\theta}{2}\right) \left(\frac{\omega}{\pi U_c}\right) \left|\mathscr{I}\left(\frac{\omega}{U_c}\right)\right|^2 \frac{a_0(\omega\delta_*/U)}{[\alpha_p^2 + (\omega\delta_*/U)^2]^{3/2}},$$

$$\alpha_0 = 0{\cdot}035, \tag{28}$$

where $M = U/c_0$ is the Mach number of the main stream, and we have introduced the approximation $U_c \approx 0{\cdot}7U$; μ is given by equation (16).

The solid curve in Figure 3 is a non-dimensional plot of the acoustic pressure spectrum for the particular case $h = \delta$, when the thickness of the turbulent boundary layer over the upper surface is just equal to the airfoil thickness h. At very low frequencies (when $\omega h/U_c \ll 1$) the radiation must be similar to that from the edge of a thin rigid half-plane. In this limit

$$\mathscr{I}\left(\frac{\omega}{U_c}\right) \sim \frac{e^{-i\pi/4}}{\mu} \sqrt{\frac{\pi U_c}{\omega + i0}}, \qquad \frac{\omega h}{U_c} \ll 1 \tag{29}$$

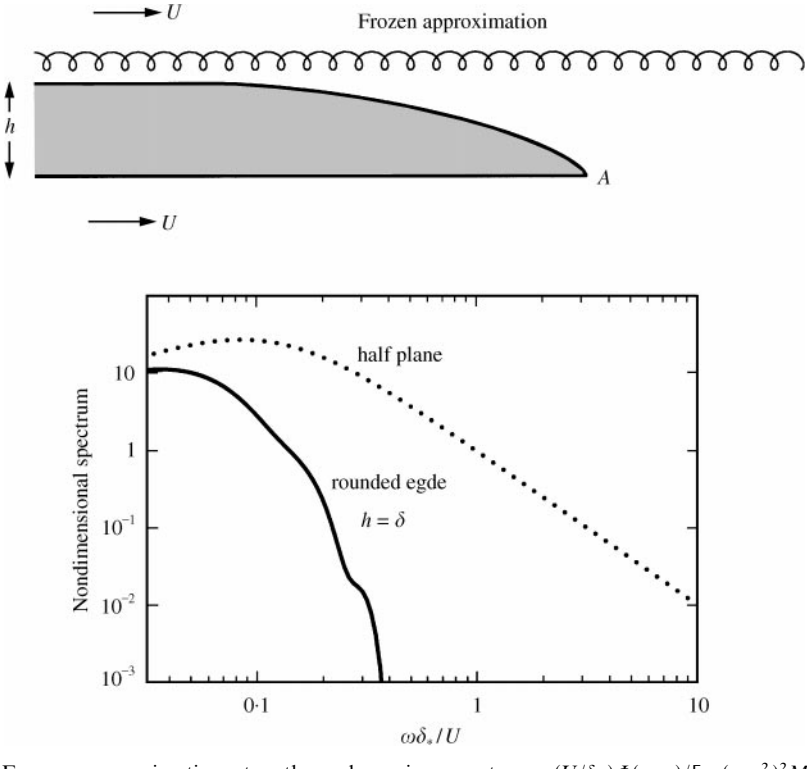

Figure 3. Frozen approximation to the edge-noise spectrum $(U/\delta_*)\Phi(\mathbf{x},\omega)/[a_0(\rho_0 v_*^2)^2 M(L\delta_*/|\mathbf{x}|^2) \sin\psi \sin^2(\theta/2)]$ for the rounded edge of Figure 2(a) of thickness $h = \delta$ when $\ell = 4h$, and for the rigid half-plane ($h = 0$).

and the spectrum becomes identical with that for the half-plane,

$$\frac{(U/\delta_*)\Phi(\mathbf{x},\omega)}{(\rho_0 v_*^2)^2} \approx M\left(\frac{L\delta_*}{|\mathbf{x}|^2}\right)\sin\psi\sin^2\left(\frac{\theta}{2}\right)\frac{a_0(\omega\delta_*/U)}{[\alpha_p^2+(\omega\delta_*/U)^2]^{3/2}} \tag{30}$$

which is also plotted in Figure 3.

The large difference at high frequencies between the half-plane and rounded edge spectra occurs because, in the frozen approximation the perpendicular stand-off distance of the separation streamline from the edge A (where the high-frequency noise is generated) is equal to the plate thickness h, so that the upwash velocity at the edge is reduced by a factor of order $e^{-|\omega|h/U_c} \ll 1$ relative to the half-plane.

3.3. FULLY ATTACHED EDGE FLOW

When the turbulent boundary layer remains attached to the curved upper surface of the airfoil right up to the edge A, as indicated in Figure 4, we write the representation (17) for $\hat{\Psi}(x_1, x_2, \omega)$ on the *upper* surface in terms of $(s, s_\perp)$ in the form

$$\hat{\Psi}(s, s_\perp, \omega) = \int_{-\infty}^{\infty} \mathscr{A}(k\,\omega)e^{iks-|k|s_\perp}\,dk, \quad s_\perp \leqslant 0,\ \zeta < 1. \tag{31}$$

$\mathscr{A}(k, \omega)$ is determined by assuming that the wall-pressure Fourier transform $p_s(k, 0, \omega)$ is defined *locally* on the curved surface, with local statistical properties defined as in equations

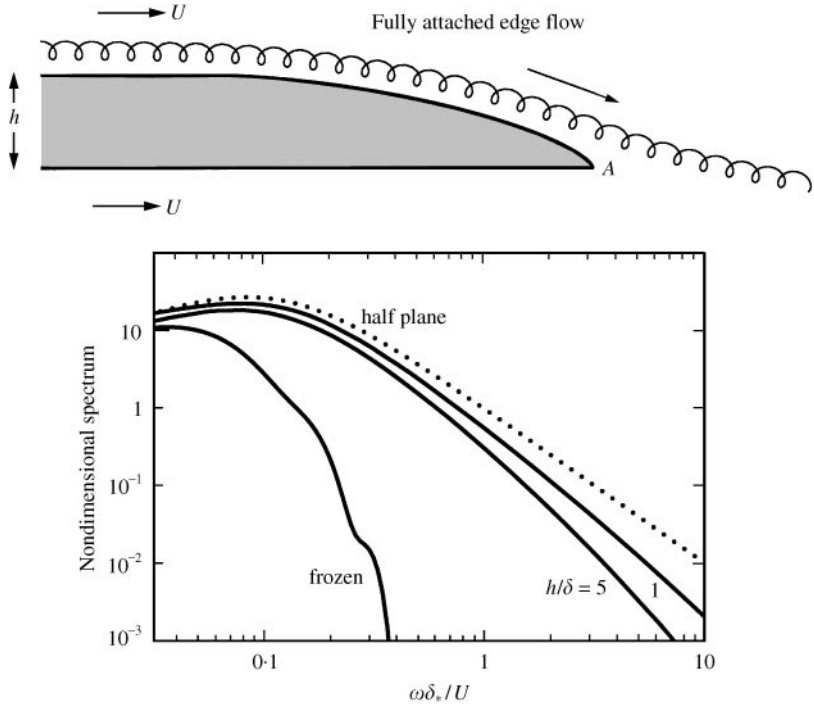

Figure 4. Predicted edge-noise spectrum $(U/\delta_*)\Phi(\mathbf{x}, \omega)/[a_0(\rho_0 v_*^2)^2 M(L\delta_*/|\mathbf{x}|^2)\sin\psi\sin^2(\theta/2)]$ for the rounded edge of Figure 2(a) of thickness $h/\delta = 1$ and 5, when $\ell = 4h$. Also shown for comparison are the frozen and half-plane spectra.

(23)–(26) that may vary over length scales much larger than the correlation scale of the turbulence.

This approximation can be used to evaluate the portion $\int_{-\infty}^{1} \hat{\Psi}(s(\zeta), 0, \omega)\,\mathrm{d}\zeta$ of the integral in the representation (12) of the sound pressure. On the lower surface of the airfoil (i.e., for $1 < \zeta < +\infty$), we apply a local plane wave approximation to equation (31) by writing

$$\hat{\Psi}(s, 0, \omega) = \int_{-\infty}^{\infty} \mathscr{A}(k, \omega) \mathrm{e}^{\mathrm{i}k\{s'(\zeta) + h'(\zeta)\sin\vartheta\} - |k|h'(\zeta)\cos\vartheta}\,\mathrm{d}k, \quad s_\perp = 0,\ \zeta > 1, \tag{32}$$

where for a point on the lower surface specified by $\zeta (1 < \zeta < +\infty)$, $s'(\zeta)$ is the value of s at the *corresponding point on the upper surface* (i.e., where the perpendicular from the lower surface point meets the upper surface), $h'(\zeta)$ is the airfoil thickness at that point, and $\vartheta = \vartheta(\zeta)$ is the angle between the $s_\perp$-axis and the x_2 *direction at the upper surface point. Thus, when* $\mathscr{A}(k, \omega)$ is approximated in terms of the blocked pressure as in equation (18), the farfield sound is found to be given by

$$p(\mathbf{x}, t) \approx \frac{-\mu \sin^{1/2}\psi \sin(\theta/2)}{|\mathbf{x}|\sqrt{2\pi c_0}} \iint_{-\infty}^{\infty} \mathrm{d}k\,\mathrm{d}\omega \int_{-\infty}^{1} \mathrm{sgn}(k)\sqrt{\mathrm{i}\omega} p_s(k, 0, \omega) \mathrm{e}^{\mathrm{i}ks(\zeta)}$$

$$\times \left[1 + \left(\frac{\mathrm{d}\bar{\zeta}}{\mathrm{d}\zeta}\right) \mathrm{e}^{\mathrm{i}kh'(\bar{\zeta})\sin\bar{\vartheta} - |k|h'(\bar{\zeta})\cos\bar{\vartheta}}\right] \mathrm{e}^{-\mathrm{i}\omega(t - |\mathbf{x}|/c_0)}\,\mathrm{d}\zeta, \tag{33}$$

where for $-\infty < \zeta < 1$, $\bar{\zeta}(\zeta)$ is the point of intersection with the lower surface of the perpendicular onto the latter from the point ζ on the upper surface, so that $1 < \bar{\zeta} < +\infty$, and $\bar{\vartheta} = \vartheta(\bar{\zeta})$.

Thus, forming the acoustic pressure frequency spectrum, as in section 3.2, we obtain the following modified form of equation (24):

$$\Phi(\mathbf{x}, \omega) \approx \frac{\mu^2 \sin\psi \sin^2(\theta/2)}{2\pi^2 |\mathbf{x}|^2} \frac{\omega L}{c_0} \int_{-\infty}^{\infty} \mathrm{d}k \iint_{-\infty}^{1} P(k, 0, \omega) \mathrm{e}^{\mathrm{i}k\{s(\zeta) - s(\zeta')\}}$$

$$\times \left[1 + \left(\frac{\mathrm{d}\bar{\zeta}}{\mathrm{d}\zeta}\right) \mathrm{e}^{\mathrm{i}kh'(\bar{\zeta})\sin\bar{\vartheta} - |k|h'(\bar{\zeta})\cos\bar{\vartheta}}\right] \left[1 + \left(\frac{\mathrm{d}\bar{\zeta}'}{\mathrm{d}\zeta'}\right) \mathrm{e}^{\mathrm{i}kh'(\bar{\zeta})\sin\bar{\vartheta}' - |k|h'(\bar{\zeta})\cos\bar{\vartheta}'}\right] \mathrm{d}\zeta\,\mathrm{d}\zeta',$$

$$|\mathbf{x}| \to \infty. \tag{34}$$

We can take account of slow changes (on a scale of the boundary layer thickness δ) in the mean properties of the boundary layer turbulence with curvilinear distance along the airfoil by permitting $P(k, 0, \omega)$ in equation (34) to be a slowly varying function of $s = s(\zeta)$ and $s' = s(\zeta')$. The simplest way to do this is to use a modified form of the Corcos approximation (25) in which the point pressure frequency spectrum $\Phi_{pp}(\omega)$ is replaced by the geometric mean $\sqrt{\Phi_{pp}(s, \omega)\Phi_{pp}(s', \omega)}$ of the corresponding spectra at s and s', namely,

$$P(k, k_3, \omega) = \sqrt{\Phi_{pp}(s, \omega)\Phi_{pp}(s', \omega)}\, \frac{\ell_1}{\pi[1 + \ell_1^2(k - \omega/U_c)^2]} \frac{\ell_3}{\pi[1 + \ell_3^2 k_3^2]}. \tag{35}$$

This would be appropriate if variations in the convection velocity $U_c \approx 0{\cdot}7U$ are small compared with changes in the structure of the point pressure spectrum Φ_{pp} as the trailing edge is approached. It is necessary to take the geometric mean (as opposed to, say, the arithmetic mean) to ensure that the right-hand side of equation (34) remains positive definite.

Thus, when the wavenumber integral in equation (34) is evaluated as before, by taking the first term in the expansion about the convective peak at $k = \omega/U_c$, we find

$$\Phi(\mathbf{x}, \omega) \approx \frac{0{\cdot}7\mu^2 LM \sin\psi \sin^2(\theta/2)}{\pi^2 |\mathbf{x}|^2} |\mathscr{F}(\omega)|^2, \quad |\mathbf{x}| \to \infty,$$

$$\mathscr{F}(\omega) = \int_{-\infty}^{1} \sqrt{\Phi_{pp}(s, \omega)} \left[1 + \left(\frac{\mathrm{d}\bar{\zeta}}{\mathrm{d}\zeta}\right) \mathrm{e}^{\mathrm{i}kh'(\bar{\zeta})\sin\bar{\vartheta} - |k|h'(\bar{\zeta})\cos\bar{\vartheta}}\right] \mathrm{e}^{\mathrm{i}ks(\zeta)}\, \mathrm{d}\zeta. \tag{36}$$

In the numerical results to be given below we shall ignore the dependence of $\Phi_{pp}(s, \omega)$ on s. In that case the acoustic pressure spectrum has the form given previously in equation (28), with

$$\mathscr{I}(k) = \mathrm{sgn}(k) \int_{-\infty}^{1} \left[1 + \left(\frac{\mathrm{d}\bar{\zeta}}{\mathrm{d}\zeta}\right) \mathrm{e}^{\mathrm{i}kh'(\bar{\zeta})\sin\bar{\vartheta} - |k|h'(\bar{\zeta})\cos\bar{\vartheta}}\right] \mathrm{e}^{\mathrm{i}ks(\zeta)}\, \mathrm{d}\zeta. \tag{37}$$

This integral must be evaluated numerically. In doing this it has been assumed that the separation streamline at the edge makes an angle $-\pi/4$ with the positive direction of the x_1-axis, which is the same as for potential flow past the airfoil when the Kutta condition is applied at A (see Part 1). In order to achieve this smooth behavior, we have set $\bar{\vartheta} = \pi/4$ at those points very close to A where the geometrical value of the angle actually exceeds $\pi/4$.

The acoustic pressure frequency spectrum is given by equation (28). It is plotted in Figure 4 for $h/\delta = 1$ and 5. The intensity of the sound decreases as h/δ increases, because the exponential decay of the second term in the square brackets of equation (37) rapidly reduces the contribution from the lower surface. However, the full effect of scattering by the upper surface is always present, so that the overall reductions with increasing thickness are very much less than those predicted by the frozen approximation.

3.4. SEPARATED EDGE FLOW

When the boundary layer separates at some intermediate point on the curved section of the trailing edge (Figure 5) the radiation can be estimated by combining the approximations of sections 3.2 and 3.3. Let separation occur at $x_1 = x_0$ ($\zeta = \zeta_0$), at the point where the airfoil thickness is h_0, and assume that immediately after separation the turbulence convects in a frozen pattern parallel to the undistrubed mean stream. In the simplest approximation in which the dependence of $\Phi_{pp}(s, \omega)$ on s is again ignored, the acoustic pressure spectrum can be set in the form (28), where

$$\mathscr{I}(k) = \mathrm{sgn}(k) \left\{ \int_{-\infty}^{\zeta_0} \left[1 + \left(\frac{\mathrm{d}\bar{\zeta}}{\mathrm{d}\zeta}\right) \mathrm{e}^{\mathrm{i}kh'(\bar{\zeta})\sin\bar{\vartheta} - |k|h'(\bar{\zeta})\cos\bar{\vartheta}}\right] \mathrm{e}^{\mathrm{i}ks(\zeta)}\, \mathrm{d}\zeta. \right.$$

$$\left. + \int_{\zeta_0}^{1} \left[\mathrm{e}^{-|k|\mathrm{d}(\zeta)} + \left(\frac{\mathrm{d}\bar{\zeta}}{\mathrm{d}\zeta}\right) \mathrm{e}^{-|k|h_0}\right] \mathrm{e}^{\mathrm{i}k(s_0 + x_1 - x_0)}\, \mathrm{d}\zeta \right\}, \tag{38}$$

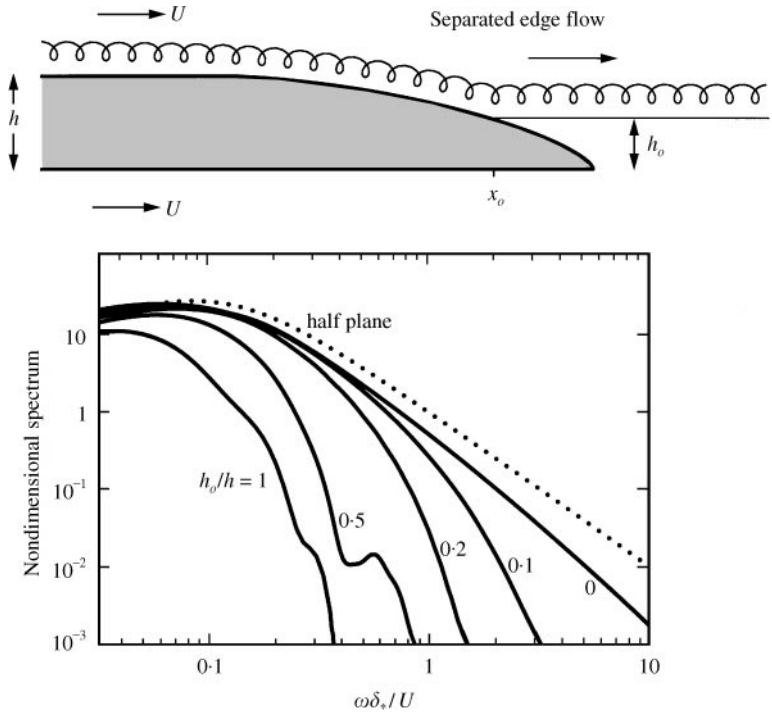

Figure 5. Predicted edge-noise spectrum $(U/\delta_*)\Phi(\mathbf{x}, \omega)/[a_0(\rho_0 v_*^2)^2 M(L\delta_*/|\mathbf{x}|^2)\sin\psi \sin^2(\theta/2)]$ for the rounded edge of Figure 2(a) of thickness $h/\delta = 1$, $\ell = 4h$, and for the separated edge flows of Table 1.

TABLE 1

Separation co-ordinates for $\alpha = 600$, $\beta = 86{\cdot}9370$

h_0/h	x_0/h	Curvilinear distance/h
1	−4	4·19
0·5	−0·97	1·11
0·2	−0·24	0·32
0·1	−0·08	0·13

where $d(\zeta) = h_0 - \frac{1}{2}h - x_2(\zeta)$ $(\zeta < 1)$ is the vertical standoff distance of the separation streamline from the upper surface of the airfoil, and $s_0 = s(\zeta_0)$. The separation co-ordinate x_0 and the curvilinear distance of the separation point from the edge are displayed in Table 1.

Typical acoustic pressure frequency spectra, calculated from the general formula (28), are illustrated in Figure 5 for the cases of Table 1 when $\delta = h$. The contributions at high frequencies decay very rapidly as the separation point moves upstream from the edge, for the reasons discussed in section 3.2. The case $h_0/h = 1$ coincides with the frozen approximation of section 3.2.

These results (and the frozen approximation of section 3.2) take no account of the sound generated by turbulence in the "dead water" region bounded by the separation streamline and the curved section of the upper surface between the separation point and the edge.

4. CONCLUSION

The intensity of the high-frequency sound generated by turbulent flow past the trailing edge of an airfoil is significantly reduced if separation occurs upstream of the geometrical edge. Separated flow over a curved trailing edge profile (Figure 5) can be modelled by assuming that after separation boundary layer eddies are convected along a path parallel to the undisturbed mean stream, so that their distance of closest approach to the sharp trailing edge is just equal to the airfoil thickness at the separation point. The strength of the unsteady interaction responsible for sound generation then decreases exponentially with increasing frequency, and predicted levels of edge noise are significantly smaller than estimates made by modelling the interaction in terms of a rigid half-plane. This conclusion ignores possible contributions to sound generation from turbulence in the recirculating zone between the separation streamline and the curved section of the upper surface between the separation point and the edge, which are probably significant only at much lower frequencies [2].

When the mean flow remains attached right up to the trailing edge, boundary layer turbulence on the suction side of the airfoil always interacts strongly with the edge. However, because of the finite thickness of the airfoil, the influence of the (turbulence free) lower surface on the radiated intensity continues to decrease exponentially fast at high frequencies. In consequence, most of the high-frequency radiation is associated with the flow interacting with the upper surface. The sound levels are smaller than for the half-plane model, but the differences at higher frequencies are more modest, typically being of the order 5–10 dB, the precise values being dependent on the ratio of the boundary layer thickness to the mean airfoil thickness.

ACKNOWLEDGMENT

The work reported here is supported by the Office of Naval Research Under Grant N00014-98-1-0798 administered by Dr L. Patrick Purtell. The author gratefully acknowledges the benefit of discussions with Dr William K. Blake during the preparation of this paper.

REFERENCES

1. M. S. HOWE 1999 *Journal of Sound and Vibration* **225**, 211–238. Trailing edge noise at low Mach numbers.
2. W. K. BLAKE and J. L. GERSHFELD 1989 *Lecture Notes in Engineering* 46 (M. Gad-el-Hak, editor). Frontiers in experimental fluid mechanics: the aeroacoustics of trailing edges.
3. W. K. BLAKE 1983 *Proceedings of the International Symposium on Turbulence Induced Vibrations and Noise of Structures* (M. M. Sevik, editor), 45–65. New York: American Society of Mechanical Engineers. Excitation of plates and hydrofoils by tailing edge flows.
4. J. GERSHFELD, W. K. BLAKE and C. W. KNISELY 1988 *American Institute of Aeronautics and Astronautics Paper* 88-3826-CP. Trailing edge flow and aerodynamic sound.
5. H. LAMB 1932 *Hydrodynamics*. Cambridge: Cambridge University Press, 6th edition; reprinted 1993.
6. D. M. CHASE 1972 *Journal of the Acoustical Society of America* **52**, 1011–1023. Sound radiated by turbulent flow off a rigid half-plane as obtained from a wavevector spectrum of hydrodynamic pressure.
7. K. L. CHANDIRAMANI 1974 *Journal of the Acoustical Society of America* **55**, 19–29. Diffraction of evanescent waves, with applications to aerodynamically scattered sound and radiation from unbaffled plates.

8. D. M. CHASE 1975 *American Institute of Aeronautics and Astronautics Journal* **13**, 1041–1047. Noise radiated from an edge in turbulent flow.
9. D. M. CHASE, 1980 *Journal of Sound and Vibration* **70**, 29–67. Modeling the wavevector–frequency spectrum of turbulent boundary layer wall pressure.
10. G. M. CORCOS, 1964 *Journal of Fluid Mechanics* **18**, 353–378. The structure of the turbulent pressure field in boundary layer flows.